MAPPING CHAPARRAL IN THE SANTA MONICA MOUNTAINS USING MULTIPLE ENDMEMBER SPECTRAL MIXTURE MODELS

Roberts, D.A.[1], Gardner, M. [1], Church, R. [1], Ustin S. [2], and Scheer G. [2]
and Green R.O. [13]

1 Department of Geography, EH3611, University of California, Santa Barbara, CA 93106
2. Department of Land, Air, and Water Resources, University of California, Davis, CA 95616
3. Jet Propulsion Laboratory, 4800 Oak Grove Dr. Pasadena, CA 91109

Submitted to

Remote Sensing of Environment

May 10, 1996

For future correspondence contact:

Dar A. Roberts
Dept. of Geography, Ellison Hall 3611,
University of California
Santa Barbara, CA 93106.
Phone: 805-893-2276
Fax: 805-893-3146
email: dar@geog.ucsb.edu

ABSTRACT

A new technique, called multiple endmember spectral mixture analysis (MESM) was developed and tested in the Santa Monica Mountains, using Airborne Visible/Infrared Imaging Spectrometer (AVIRIS) data acquired in the fall of 1994 to map California chaparral. The technique models remotely measured spectra as linear combinations of pure spectra, called endmembers, while allowing the types and number of endmembers to vary on a per pixel basis. In this manner, vegetation is characterized by a unique set of endmembers as well as by the fractions. Reference endmembers were selected from a library of field and laboratory measured spectra of leaves, canopies, non-photosynthetic materials (e.g. stems) and soils and used to develop a series of candidate models. Each candidate model was applied to the image, then, on a per pixel basis, assessed in terms of fractions, root mean squared (RMS) error and residuals. If a model met all criteria, it was listed as a candidate for that pixel. For this study, selection criteria included fractions between -0.01 and 1.01, an RMS less than 0.025 and a residual less than 0.025 in seven or more contiguous bands. A total of 889 two-endmember models were evaluated and used to generate 276 three-endmember models. To facilitate model selection from a large pool of candidates, an optimal set was selected to provide maximal areal coverage. A total of 24 two-endmember and 12 three-endmember models were chosen. These models were used to generate fraction images and vegetation maps showing evergreen and drought deciduous or senesced vegetation.

We found that a majority of the image could be modeled as two-endmember models. Three-endmember models provided greater areal coverage, yet provided poorer vegetation discrimination due to an increase in model overlap (two or more model candidates modeling the same pixel). The vegetation maps demonstrate that the technique is capable of discriminating a large number of spectrally distinct types of vegetation while

capturing the mosaic-like spatial distribution typical of chaparral. However, additional research is required to fully evaluate the technique and validate the vegetation maps that were produced.

INTRODUCTION

California chaparral is the most extensive type of natural vegetation in Southern California (Wieslander and Gleason, 1954) where it represents a significant source of species diversity (Hanes, 1977) and plays a major role in ecosystem dynamics due to its unique fire ecology (Keeley and Keeley, 1988). The abundance of chaparral along the wildland urban interface and the high fire hazard it represents, provide extra incentives for mapping and management of chaparral communities. Management problems have been further magnified by nearly seventy years of fire suppression and drought related die-back over the last few years resulting in a large accumulation of highly combustible fuels (Radtke et al., 1982; Yool et al., 1985).

Remote sensing represents one means for rapid, regional mapping of chaparral. However, mapping is complicated by the complex spatial distribution of chaparral which, in response to steep topographic gradients, harsh edaphic conditions and variable fire histories, typically forms a complex mosaic of different species dominants and age classes, each with unique successional responses to fire and canopy characteristics (e.g. moisture content, biomass, fuel load). Previous attempts at mapping chaparral using remote sensing have met with variable success. For example, efforts using the Landsat Multispectral Scanner (MSS) resulted in poor separation of shrub communities (Nichols, 1974; Estes et al., 1981). Additional studies have combined collateral information such as topographic data with remote sensing (Shasby et al., 1981) providing improved results (Cosentino et al., 1981).

In this study, we investigate the use of the Airborne Visible/Infrared Imaging Spectrometer (AVIRIS) for providing improved maps of chaparral. We have developed, and teste, a new algorithm for mapping vegetation, in which remotely measured data are modeled as linear spectral mixtures where the number of pure components (endmembers), and types of components vary across the image. In this manner, chaparral communities may be distinguished both on the basis of the relative proportions of the endmembers as well by community specific endmember selection. This research represents a part of a larger on-going collaborative study with the Los Angeles County Fire Department (LACFD) and United States Forest Service (USFS) to provide improved maps of chaparral for fire prediction and preventive modeling.

MATERIAL and METHODS

Study Site

The study was initiated in the Santa Monica Mountains, an east-west trending range that extends approximately 73 km from the Oxnard alluvial plain in the west to the Los Angeles river in the east, with elevations ranging from sea level to as high as 949 m at Sandstone Peak. Annual precipitation is low and temperatures moderate, varying seasonally between hot, dry summers and cool wet winters typical of Mediterranean climates. Geologically, the Santa Monica Mountains represent the most variable portion of the transverse range, consisting primarily of Miocene marine shales and breccias and extensive volcanic rocks including dikes, sills and andesitic, diabasic and basaltic flows (Norris and Webb, 1990). In the east, the rocks consist primarily of Cretaceous marine sandstone and shale and Paleocene marine limestone and shale. Late Eocene nonmarine flood plain deposits are scattered throughout the range. Uplift and erosion of the range have been relatively recent occurring in the Pliocene and Quaternary (Dibblee, 1982).

Climatic, edaphic (e.g. substrate) and topographic factors combine to produce a complex mosaic of diverse vegetation including at least four distinct types of chaparral (chamise, Ceanothus, mixed and redshanks), wetlands, riparian habitats, woodlands, and coastal sage scrub. Vegetation patterns are complicated by the complex fire history and resulting diversity in successional states of the vegetation. For example, between 1935 and 1994 over 115 fires larger than 16 ha were recorded for the general region (Office of Emergency Services, 1995) with some areas experiencing multiple burn events.

Intermingled with this complex landscape of natural vegetation is an equally complicated mosaic of land ownership and land use; the Santa Monica National Recreation Area (SMNRA) consists of ~62,750 ha, of which 27,900 are privately owned, and the remainder are distributed amongst the National Park Service (7,280), State Park system (23,500) and Los Angeles County or municipal parks (4,050). The diversity of vegetation, complex land-use patterns and high frequency of fires make the Santa Monica Mountains an ideal study site for mapping chaparral because of the real need for improved fire hazard assessment and improved management for fire and biodiversity.

Data Acquisition and Preprocessing

Analysis focused on AVIRIS data collected on October 19, 1994. AVIRIS is an imaging spectrometer that collects spectra at a nominal full-width half maximum and sampling interval of 10 nm resulting in 224 spectral bands between 370 and 2500 nm. It is flown on the ER-2 at an elevation of 20,000 meters, collecting a cross track swath of ~ 11 km, with a ground instantaneous field of view of 17.4 m for this flight. A typical scene consists of 614 samples, and 512 lines, covering a 11x 9 km area. Two east-west flight lines were acquired, consisting of a total of 12 scenes. Results will only be presented for flight 941019D, run 3, scene 5, centered over Point Dume, California (Fig. 1). Areas labeled as Zuma and Castro on the figure show the location of two field sites, one

consisting of coastal sage scrub (Zuma) and the other chamise (Castro), where plant samples and canopy scale field spectra were measured. Maps of equivalent liquid water thickness, precipitable water vapor and apparent reflectance were generated using an algorithm coupled with the Modtran3 radiative transfer code (Green et al., 1993; this issue). Apparent reflectance spectra for three vegetation types identified in the field including chamise (labeled as Adenostoma), Ceanothus and coastal sage scrub, are plotted to the left of the index map (Fig.1).

Figure 1

Once converted to apparent reflectance, the AVIRIS data were modeled as spectral mixtures of field and laboratory measured spectra of soil, non-photosynthetic vegetation (NPV), green leaves and shade (Adams et al., 1993; Roberts et al., 1993). Spectral mixture analysis (SMA) was performed using a multiple endmember spectral mixture model (MESM), in which the number of endmembers and types of endmembers are varied across the image (e.g. Roberts et al., 1992). The MESM approach will be described in more detail below.

Endmembers were selected from a spectral library consisting of 889 field and laboratory measured reflectance spectra. Laboratory measured spectra included a selection of green leaves, senesced materials, stems and soils measured at the University of Washington prior to 1991 and a second selection collected in the Santa Monica Mountains in the spring and fall of 1995 that were measured at the University of California, Davis (see Ustin et al., this issue for a description of the sites and sampling techniques). At the University of Washington, hemispherical reflectance was measured using a modified Beckman DK2a with an integrating sphere attachment. At the University of California, spectra were measured with a Cary-5E (Varian, Inc. Sunnyvale,

CA). All spectra were standardized to halon then convolved to the band pass and wavelength interval for the October 1994 AVIRIS flight.

Field spectra were collected at three field sites in the Santa Monica Mountains: Zuma, Castro (Fig. 1) and a third site near Encino reservoir consisting of a high biomass stand of Ceanothus. These spectra were collected using an Analytical Spectral Devices full range spectrometer (Analytical Spectral Devices, Boulder, CO) and standardized to spectralon (Labsphere, Inc., North Sutton, NH). They were collected from a cherry picker on loan from the LACFD at a height ranging from 3 to 5 meters above the canopies. Prior to data collection 7 to 8 individual shrubs were flagged at each site. The bucket was positioned above each shrub, the height of the bucket recorded and a photograph taken to ensure accurate relocation. Spectra were collected at roughly one hour intervals from close to solar noon to near sunset (4 to 7 collections). These sites were visited in the spring (June 8-10) and revisited in the fall of 1995 (October 16-18). Field spectra were then convolved to the October 1994 wavelengths and combined with the laboratory spectra. Finally, atmospheric and instrumental artifacts were removed by selecting bands outside of the major water vapor absorption regions, resulting in a 179 band subset of the original 224 bands.

Spectral Mixture Analysis

AVIRIS apparent reflectance spectra were modeled as linear combinations of two or more spectra selected from the spectral library. A spectral mixture model is a physically based model in which a mixed spectrum is modeled as a combination of pure spectra, called endmembers (Adams et al., 1993). When photons interact with a single component within the field of view, the mixture can be modeled as a linear sum of each component weighted by the proportion of the components within the field of view. When scattered photons interact with multiple components, such as multiple NIR scattering by

vegetation, the mixture has the potential of becoming non-linear (Johnson et al., 1983; Shipman and Adams, 1987; Roberts et al., 1993). For most applications, multiple scattering is assumed to be negligible, although for a variety of vegetation, non-linearity has been shown to be significant (Huete, 1986; Roberts et al., 1993; Borel and Gerstl, 1994; Ray and Murray, 1996). Example applications of linear mixture models include Graetz and Gentle (1982), Pech et al. (1986), Smith et al. (1990a & b), Adams et al. (1993), Roberts et al. (1993) and Shimabukuro et al. (1994). In this paper we assume linear mixing.

The linear mixture model is based on the fundamental equation:

$$P_{i\lambda}' = \sum_{k=1}^{N} f_{ki} * P_{k\lambda} + \varepsilon_{i\lambda} \quad \text{and} \quad \sum_{k=1}^{N} f_{ki} = 1 \qquad (1)$$

Where a spectral mixture, $P_{i\lambda}'$ from location **i**, is modeled as the sum of **N** reference endmembers, $P_{k\lambda}$, each weighted by fraction f_{ki}. Unmodeled portions of the spectrum are expressed as a residual term, $\varepsilon_{i\lambda}$, at wavelength λ. In this analysis, fractions were constrained to sum to 1.0 and were derived using modified Gramm-Schmidt orthogonalization (Adams et al., 1993). Model fit is assessed either using the residual term, $\varepsilon_{i\lambda}$, or via a Root-Mean Squared Error (RMS) (Eq. 2):

$$RMS = \sum_{k=1}^{N} \text{sqrt}(\Sigma(\varepsilon_{i\lambda})^2)/(N-1) \qquad (2)$$

In the terminology used by Gillespie et al. (1990) and Adams et al. (1993), endmembers can be derived from the image (image endmembers) or derived from a

library or field reflectance spectra (reference endmembers). Analysis in this paper is based on reference endmembers. One standard application of SMA is to select an optimal set of reference endmembers, typically including green vegetation (GV), soil, NPV and shade, that minimize the RMS and residual errors, and provide reasonable (positive and physically meaningful) fractions throughout most of the image (Smith et al., 1990a & b). This approach has an advantage in that it is relatively simple and provides a physically meaningful measure of abundance that is portable across sensors and through time (e.g. Adams et al., 1995; Roberts et al., 1996). However, there are a number of disadvantages to the simple mixing concept.

The simple mixing model concept is limited because it fails to account for the fact that the number of materials within the field view and the spectral contrast between those materials is variable. For example, a forested ecosystem might be best described as a mixture of green leaves and shade while a shrubland may require four. According to Sabol et al. (1992), the accuracy of fractions will be highest when the exact number that are required to account for the spectral variability are utilized in the model; too few endmembers will partition the unmodeled endmember into the fractions (creating a fraction error) and increase the RMS; too many endmembers will make the model sensitive to instrumental noise, atmospheric contamination and natural variability in spectra, resulting in fraction errors. Fraction errors are commonly expressed as negative fractions in models that are unconstrained to force positive fractions. Even with 224 channels, the high degree of correlation between each wavelength results in fairly low dimensionality for any given pixel.

Another disadvantage to the simple mixing model concept is that it fails to account for subtle spectral differences between materials that will have little impact on RMS error and will only be expressed in the fractions and/or as a residual. For example,

Roberts et al. (1993) found that senesced grass and soils were difficult to include in the same mixture model without generating fraction errors but could readily be distinguished by mapping ligno-cellulose absorptions expressed as residuals from a three endmember model that excluded NPV. This concept can further be illustrated by comparing two laboratory measured leaf spectra (Sophora, Grassme1) to a spectrum of chamise (Castro) derived from the Santa Monica AVIRIS data (Fig 2a). The AVIRIS spectrum can be modeled as a mixture of photometric (spectrally flat) shade and either leaf spectrum. In the case of "Sophora", a high reflectance leaf, chamise is modeled as having a lower GV fraction (0.42), while the lower reflectance leaf, "Grassme1", results in a higher GV fraction. Of these two models, "Sophora" would be selected as a better model based on a lower RMS error (0.019) and lower residuals (Fig. 2b). In a four-endmember model, residuals and RMS errors would be expected to drop significantly, making the two models distinguishable primarily as a difference in the GV and shade fractions.

Figure 2

In this paper we develop a new technique that minimizes fraction errors while permitting a larger number of endmembers to be modeled across a scene. Using this approach, the number of endmembers, and types, are allowed to vary for each pixel in the image. The approach we have developed is an extension of previous work by Roberts et al. (1992) in which AVIRIS data were modeled by sets of two-endmember mixture models derived from the image (image endmembers). The two-endmember models were then used to construct three-endmember models. In this paper we generate sets of candidate models from reference endmembers, rather than deriving them from the image. This new approach has distinct advantages in that it is: 1) repeatable, 2) portable between images and 3) produces fraction images that are connected to the spectra of real materials.

The key to the multiple endmember approach is to start with a series of candidate two-endmember models, evaluate each model based on selection criteria then, if required, construct candidate models that incorporate more endmembers. Three selection criteria were used in this study (Fig 3). These include:

1) A fraction criterion. A model is selected only if it produces physically reasonable fractions between -0.01 and 1.01. A 1% error is permitted to allow for instrumental noise generated errors in fractions.

2) An RMS criterion. A model is selected only if the RMS is below the threshold. In this study a threshold of 0.025 was used. A lower threshold (e.g. 0.020) will reduce the likelihood that a candidate model is selected while a higher threshold will increase the likelihood.

3) A residual criterion consisting of a threshold and count. The residual threshold was established to evaluate whether any individual residual exceeds the absolute value of the threshold. The residual count was established to count the number of times the threshold was exceeded contiguously. A contiguous threshold count was used to distinguish residuals resulting from noise and atmospheric contamination from residuals resulting from the presence (or absence) of an absorption in a candidate model relative to a mixture. Through experimentation, a residual count of 7, corresponding to width of 70 nm wide, was selected.

At the extremes of threshold values, very low thresholds (small RMS, small residual and count) will produce no candidate models while large thresholds will make every model a candidate. Therefore, optimal criteria would lie somewhere between these two extremes.

The concept of multiple two-endmember models is illustrated readily by a scatterplot between 830 and 670 nm (Fig. 3). Data points from three spatially and

spectrally distinct regions are plotted as solid triangles, open diamonds and solid squares. From the point of view of a simple mixing model, these spectra could be modeled as a three endmember mixture of photometric shade, GV (Sophora) and NPV (Scpnls). Alternatively, the data could be modeled as three separate two-endmember mixture models consisting of photometric shade mixed with two types of green leaves (Sophora, Grassme1) or NPV (Scpnls). In the first approach, the vegetation type that corresponds to the open diamonds would be distinguished from vegetation shown by the solid triangles based on a higher NPV fraction. In the latter approach, each cluster would be modeled by its own unique set of endmembers.

Figure 3

The multiple endmember mixture model was implemented by constructing a library consisting of 889 candidate two-endmember models. For this study, all two endmember models were developed as a mixture of a bright endmember (GV, soil or NPV) and photometric shade. Candidate models were constrained to have fractions between -0.01 and 1.01, an RMS threshold below 0.025, a residual threshold of 0.025 and a residual count of 7. A program was designed that produced an output image consisting of up to 1000 bands, each band corresponding to a candidate model. If a model met the criteria it was assigned a value of 1 in the matrix, 0 otherwise. Each model was evaluated for each pixel, representing in this study 889 separate mixture models for each of the 314,368 pixels in an AVIRIS scene. Ocean pixels were screened based on a shade fraction of 80% or higher. Ocean was screened because it could be modeled by all 889 candidates. A subset of 24 two-endmember models were selected and used to construct 276 three-endmember models involving two high reflectance endmembers and photometric shade. Subselection is described below.

Optimization of model selection

The approach we employed requires subselection from a potentially large number of candidate models. To assign a class to each pixel it becomes necessary to choose which, among the models, represents the optimal candidate. Several steps were taken to remove poor candidates, reduce the overall number of candidates and reduce model overlap. The overall objective when evaluating candidate models was to select the smallest subset (between 10 and 20 models) that can classify the largest area while ideally minimizing endmember model overlap. This problem can be formulated as an integer programming problem that mimics the classical maximal covering problem of Church and Revelle (1974). To formulate the problem we define the following:

i, I = index and a representative sample set of pixels from the scene to be used to in selecting an optimal set of models.

j, J = index and set of potential endmember models

α_{ij} = 1 or 0, 1 if pixel i can be classified by model j, 0 otherwise.

p = the number of models to be chosen (10-20).

a_i = The number of pixels represented as element i, initially set to 1.

X_j = 1 or 0, 1 if model j is chosen, 0 if not.

Y_i = 1 or 0, 1 if pixel i *cannot* be classified by the selected set of models, 0 otherwise.

Our objective was to minimize the following function:

$$Z = \sum_i a_i Y_i \qquad (3)$$

Subject to the constraints that

$$\sum_j \alpha_{ij} X_j + Y_i \geq 1 \text{ for each } i \in I \qquad (4)$$

$$\sum_j X_j = p \qquad (5)$$

Two procedures were employed to solve this problem. The first was General Integer Programming using CPLEX, a commercial software package. The second was a special heuristic based on an approach developed by Church for the Maximal Covering Problem (Church and Revelle, 1974), that belongs to a class of heuristics called λ- Opt.

Before the model was solved, several steps were taken to reduce the number of candidate models and samples used in optimization. These steps involved:

Initial reduction of candidate models

1) Removing all models that accounted for less than 0.001% of the image (314 pixels out of 314,368).

2) Removal of spatially fragmented models. At the resolution of the 17.4 m AVIRIS pixel, vegetation communities would be expected to form contiguous blocks of pixels rather than single pixels scattered across the image. Candidate models that showed clustering behavior (desired) were located by running a 3x3 median filter across the image corresponding to each model (consisting of a 1 or a 0), then subtracting the filtered image from the original model. Through visual comparison it was found that a 20% loss of pixels through filtering was characteristic of a fragmented distribution. Through these two steps candidate models were reduced from 889 to 223 models.

Pixel subsampling

Because the optimization routines were computationally intensive, the images were further sampled to reduce the number of pixels evaluated by these routines. Three steps were employed for pixel reduction:

1) Pixel subsampling. The 223 candidate models were sampled every third sample and third line, producing a reduced list of 35,055 pixels.

2) Dominated models were eliminated. A dominated model was defined as a model for which every pixel could also be modeled by a different, more abundant candidate.

3) Equivalent pixels were consolidated. If a pixel could be modeled by the exact same suite of models as another pixel, the pixels were consolidated and represented as one. For example, if i and î were consolidated, then $a_i \rightarrow a_i + a_{\hat{i}}$ and pixel i was removed from the optimization problems.

RESULTS/DISCUSSION

Out of 889 candidate two-endmember models, 14 were selected that provided optimal areal coverage. These models consisted of 7 NPV and 7 GV spectra and mapped a majority of the natural vegetation in the area. At the time of the overpass, in Fall 1994, much of the natural vegetation consisted of evergreen shrubs and trees or senesced grasslands and drought deciduous sage scrub. The former were modeled as mixtures of GV and shade, the latter as mixtures of NPV and shade. This 14 model subset was expanded to include spatially contiguous regions in the image where viable two-endmember models existed, yet were not chosen because of low areal coverage. Examples of these kinds of models included roads, bare rock, beaches or spatially contiguous, yet small patches of natural or disturbed vegetation. Expansion was accomplished by removing all pixels that were modeled by the original 14 model set, then stepping through each of the remaining 209 models and selecting regions that were neglected in the optimization step. In total, 24 models were selected consisting of 10 NPV spectra, 8 GV spectra and 6 rocks/soils (Table 1). These models accounted for 185,588 pixels, representing 75% of the terrestrial area in the image. The remainder consisted of 66,656 water pixels and 62,124 (19.8%) pixels that remained unmodeled.

Table 1

These results demonstrate the large degree to which a spectral mixture can be modeled by a small number of endmembers. At the same time, they also demonstrate that no single set of endmembers can adequately describe every spectrum in the image. Although over 80% of the image could be modeled using just two endmembers, a total of 24 endmembers were mapped across the image. The degree to which these models represent spatially contiguous, potentially meaningful units across the landscape can be illustrated using a subset of three of the models (Fig. 4). In this figure, three models consisting of GV-Shade, NPV-Shade and Soil-shade are displayed as red, green, and blue, respectively. Unmodeled areas and water are displayed as black. Of these three models, the most extensively distributed is the GV-shade model. Based on field work conducted in 1995, this model roughly corresponds to the distribution of chamise (Adenostoma fasciculatum). The NPV-shade model (Scpnls) corresponds to drought deciduous sage scrub, while the Soil-shade model accurately maps major roads in the area. The purity of colors (absence of cyan, magenta or yellow), indicates very little model overlap, which was typical of most of the models selected.

Figure 4

At the same time displaying intriguing spatial patterns, the nature of the models that were selected raises important questions. Very few of these spectra are of materials located in the study area (Table 1). Of the 24 models, only six are spectra collected in the Santa Monica Mountains, of which five are of NPV and one a GV spectrum. The problem is particularly acute for GV spectra. Several of the models (e.g. Blkbrush and Purglan) are leaf spectra from desert species. Ideally, a more satisfactory model would have selected

only materials, such as Adenostoma fasciculatum, that both occur in the area and were in the library.

To a certain extent, these results reflect the fact that 1) key spectra were missing from the library and 2) the MESM and optimal area coverage approaches were unconstrained in terms of the kinds of spectra that could be selected. For example, no soil spectra were available for the area. Of the green leaf spectra, only a dozen species were represented in the library. Furthermore, had the model been limited to a regionally specific library, consisting only of materials known to be in the area, it may have provided nearly the same coverage, yet selected spectra that actually matched materials in the field of view.

The 24 two-endmember models were used to generate 276 three-endmember models consisting of a bright endmember (GV, soil, NPV) and photometric shade. After masking pixels that had already been modeled using two-endmembers, and screening for low coverage and fragmentation, these 276 models were reduced to a subset of 101 models. The top 10 models of this subset were selected based on maximal area coverage. Two additional models were selected by removing the top 10, then individually assessing the remaining 91 models and searching for spatially contiguous regions with small spatial extent. After screening and optimization, three-endmember models accounted for an additional 55,882 pixels, leaving 10,774 pixels unmodeled (Table 2). The remaining 10,774 pixels consisted of spatially contiguous areas of the image, primarily in urban areas, for which no matching spectrum existed in our library.

Table 2

These results demonstrate the extent to which even a 224 channel data set, such as AVIRIS, can be modeled using a relatively small number of endmembers. Over 96% of the image could be modeled with 3 endmembers or less. Of the three-endmember models, the most spatially extensive was a NPV-GV-shade model (29 in Table 2). A majority of the remaining three-endmember models consisted of endmembers in different categories (e.g. GV-NPV, GV-Soil etc). The exceptions were models 25 and 36 (two NPVs) and 26 (two GVs).

One key objective of this study was to investigate the use of MESM for mapping chaparral. An alternative way to view the approach is to consider MESM similar to more standard classification schemes such as cluster analysis. Unlike cluster analysis, however, classes are assigned to spectra based on whether they fall within the spectral region described by a two-endmember vector, three-endmember plane, etc. In addition, unlike cluster analysis, a pixel does not necessarily belong to a single class, but may be described by several models that fit the criteria. In this paper, we describe non-unique class assignment as model overlap.

Using the 24 two-endmember candidate models, model overlap was relatively minor. A majority of the pixels could be described by a single candidate or two overlapping models (Fig. 5). Pixels which had four or more candidates, in general, consisted either of roads, or north facing slopes, in which the low signal reduced model discrimination by lowering the RMS and residual errors. In comparison, using half as many candidates, the three-endmember models resulted in nearly twice as much overlap (Fig. 5).

Figure 5

These results suggest a strategy for improved discrimination of vegetation across the landscape. Based on a comparison of the two-endmember and three-endmember models, it could be concluded that a better strategy for mapping vegetation would be to minimize the number of endmembers used in the model. By using two-endmembers it becomes possible to attach a majority of the image to a unique mixture of shade and one of GV, NPV or soil. Using three endmembers, far less of the image is uniquely modeled. When interpreting these results, however, it is also necessary to evaluate them within the context of the criteria used to select the models. Had we lowered the RMS criterion (say to 0.02) and tightened the residual constraints, fewer two-endmember models would have been selected. Tighter constraints would also have had the effect of lowering overlap for the three endmember models.

In terms of assigning class names, model overlap presents a problem. When two models overlap, one is either forced to carry the ambiguity, or choose between the models. When choosing between competing models, one is forced to decide the order in which class names will be assigned. The choice becomes more difficult as the degree of overlap increases. Our strategy for choosing between overlapping models is discussed below.

Map Generation

The two-endmember and three-endmember models were used to generate maps showing the distribution of spectrally distinct chaparral vegetation, urban vegetation, grasslands and roads. Two maps were generated, one showing vegetation dominated by senesced grasslands and drought deciduous sage scrub (Fig. 6), the other showing vegetation dominated by evergreen shrubs and trees (Fig. 7). Class names were assigned to the names of the spectrum used in the model because many of the classes had not been

rigorously evaluated in the field. The colors associated with each class name (spectrum) are included in both figures. Because many of the models still showed overlap (more than one model assigned to a pixel) decisions had to be made concerning the order in which models would be assigned to the image. The approach taken in this study was to start by assigning class names to pixels using models that showed minimum overlap first. Where extensive model overlap occurred, pixels were assigned to the model that was less extensively distributed (representing subsets of the more extensively distributed model).

Figure 6

Figure 7

Vegetation maps produced using MESM showed that the technique is capable of mapping a large number of spatially and spectrally distinct types of vegetation. For example, 9 classes of NPV-shade models were mapped for the Santa Monica Mountains (Fig 6). Field work in the spring and summer of 1995 verified that a number of the spectral classes match distinct vegetation units. For example, class 1 (Scpnls) matches regions known to be dominated by senesced grasslands while classes 2 and 3 (Zerci2st710 and Wphlph2) match coastal sage scrub. Furthermore, the large number of classes and mosaic like distribution match what is known concerning the vegetation in the area. The map of evergreen vegetation distinguished areas known to consist of Adenostoma fasciculatum (Sophora) from areas that have been observed to consist of Ceanothus (Grassme1). Urban Vegetation (red), was mapped using three of the models, and very accurately mapped the distribution of vegetated urban areas as distinct from natural vegetation. This result alone may be of use in mapping the extent of chaparral.

Some of the classes, however, should be viewed with caution. Although a large number of vegetation classes were mapped, the extent of field work to date is not

adequate to verify how many of them correspond to real units on the ground. Regions where two or more models overlapped should, in particular, be viewed with caution. Had a different model been selected, the spatial pattern may have been very different. Finally, the names of the models that were selected provide some reason for caution. A majority of the evergreen models correspond to spectra selected from the general library, not from spectra that are specific for the area. For example, "Sophora", which roughly maps Adenostoma, was chosen over chamise spectra (at the leaf and canopy scale). Of the spectra that were selected, more than half correspond to vegetation that is known to not occur in the area. An alternative strategy would be to run the models on a smaller subset of models that consist only of materials known to be in the area. It is possible, using the maximal area coverage approach, that the models that were selected were only slightly better than models using spectra collected in the area. Had the program been given only a choice from a regionally specific library, it may have produced a similar result but used spectra of materials in the area.

In addition to vegetation maps, images were generated showing the distribution of fractions of GV, NPV, soil and shade (Fig 8). The fraction maps were generated starting with maps corresponding to the fractions of all 24 endmembers. Each fraction image was placed in its appropriate category (e.g. GV), then combined with all other endmembers in the same category. Fractions were combined at pixels where two endmembers of the same category were mapped (e.g., two GV endmembers + shade). Fraction images are displayed with NPV, GV and soil as red, green and blue (Fig. 8). Bright colors correspond to high fractions and dark colors to low fractions. All fractions remained physically reasonable, between 0 and 100%. The extent to which the image was modeled using two-endmember models is reflected in the purity of the colors. Very few pixels had significant mixtures of GV, NPV or soil. South facing slopes and ridges dominated by

NPV are displayed as bright red. South facing slopes dominated by GV are displayed as bright green. North facing slopes of either NPV or GV are shown as dark red or green.

Figure 8

The fraction image shown in Figure 8, represents only one of many ways the information could be displayed. For example, with 24 endmembers it is possible to create 24 separate fraction images, one for each endmember. When combined with the unique combination of endmembers associated with each model, this provides a very large amount of information. When merged with other AVIRIS products such as maps of liquid water and water vapor, this provides an unprecedented amount of information about the terrestrial surface. One obvious challenge will be in determining how to best organize this information to answer specific questions about a region. In this study, our primary objective was to investigate a new method for mapping California chaparral. Near term goals will be to combine our vegetation classes with other remotely measured and field measured measures of abundance, moisture content and fuel loads to provide necessary information for prediction and management of fire in the region.

SUMMARY

In this paper we describe a new technique that uses a multiple endmember spectral mixture model (MESM) to map California chaparral as linear mixtures of two or more reference endmembers. The technique has the potential for providing improved discrimination of vegetation classes through pixel-unique endmember selection while providing estimates of fractional abundance of the components within the field of view. MESM is based on the concept that, although any individual spectrum can be modeled with relatively few endmembers, the number of endmembers, and types of endmembers

are variable across an image. A subset of all possible models was selected based on optimization for maximal area coverage.

The MESM approach was applied in the Santa Monica Mountains, a topographically and geologically complex region where frequent fires and complex land-use patterns make mapping and management of California chaparral critical. Using the technique, we mapped 7 evergreen classes and 9 senesced or drought deciduous classes of natural and introduced vegetation in the area. Two-endmember models provided better separation of classes than three-endmember models because of reduced model overlap. Because the classes are attached to actual laboratory or field spectra, they are readily interpreted in terms of the types of materials within the field of view.

Although the results are very encouraging, they are still preliminary. Before the maps generated in this study can be used for applications such as fire modeling and prediction they must be validated in the field. In addition, further research is necessary to determine optimal constraints for evaluating the models. Regionally specific libraries represent a potentially fruitful direction for further research. For example, an urban library might consist of spectra of materials typically found in urban environments and used to identify and map them. In the Santa Monica Mountains, a regionally specific library for chaparral might provide a direct means for mapping assemblages of species based on improved spectral fits. Finally, techniques for minimizing model overlap and ordering of classes need further investigation.

The increasing availability of imaging spectrometry data and the long term desire of ecologists and managers to obtain detailed maps of species or species assemblages high-lite the need for new tools for analyzing multispectral data and the need for improved spectral characterization of vegetation. In this paper we present a new approach

that may provide a better link between remotely sensed data and species assemblages, better discrimination between vegetation types and the potential for mapping abundance through spectral fractions.

ACKNOWLEDGMENTS

We wish to thank Dr. Ray Sauvijot of the National Park Service in Santa Monica Mountains , Mr Jimmie Ryland, Deputy Fire Chief, and personnel of the Los Angeles County Fire District for assistance and support in this study. In addition, we wish to thank Dr. Susan Conard and Mr. John Rugglesbrugge of the U.S. Forest Service for help in selecting the field sites and organizing field activities. We thank Mr. Peter Fonda-Bonardi of the Urban Research Section of the Los Angeles County Department of Internal Services for his original interest in this research. Finally, we wish to thank Dr. John Gamon of Cal. State Los Angeles for his assistance in the field. Support for this research was provided by a grant from the National Aeronautics and Space Administration, Terrestrial Ecosystems and Biogeochemical Dynamics Branch, NAGW-4626-I, as a subcontract with U.C. Davis. Computer equipment was supplied largely as part of a start-up package at U.C. Santa Barbara in the Department of Geography.

REFERENCES

Adams, J.B., Smith, M.O. and Gillespie, A.R. (1993), Imaging spectroscopy: Interpretation based on spectral mixture analysis, In Pieters C.M., and Englert, P., eds. Remote Geochemical Analysis: Elemental and Mineralogical Composition 7: 145-166, Cambridge Univ. Press., NY.

Adams, J.B., Sabol, D., Kapos, V., Almeida Filho, R., Roberts, D.A., Smith, M.O., Gillespie, A.R.(1995), Classification of Multispectral Images Based on Fractions of

Endmembers: Application to Land-Cover Change in the Brazilian Amazon, *Rem. Sens. Environ,* 52:137-154.

Borel, C.G., and Gerstl, S.A.W. (1994), Nonlinear spectral mixing models for vegetative and soil surfaces, *Remote Sens. Environ.* 47:403-416.

Church, R., and Revelle, C., (1974), The maximal covering location problem, *Papers of the regional science division,* 2: 101-118.

Cosentino, J.J., Woodcock, C.E., and Franklin, J., (1981), Scene analysis for wildland fire-fuel characteristics in a Mediterranean climate., In *Proc. 15th Int. Symp. Remote Sens. Environ.* 2: 635-643.

Dibblee, T.W., (1982), Geology of the Santa Monica Mountains and Simi Hills, Southern California, pp. 94-130, In *Geology and Mineral wealth of the California Transverse Ranges*, South Coast Geological Society.

Estes, J., Strahler, A., Cosentino, M., Woodcock, C., and Franklin, J., (1981) USFS vegetative fuels research Final Report, USFS Grant 53-91S8-06411, March 1981, 20p.

Gillespie, A.R., Smith, M.O., Adams, J.B., Willis, S.C., Fischer, A.F., and Sabol, D.E., (1990), Interpretation of residual images: spectral mixture analysis of AVIRIS images, Owens Valley, California, In *Proc. 2nd Airborne Visible/Infrared Imaging Spectrometer (AVIRIS) Workshop* (R. Green Ed.), Pasadena, CA, June 4-5, 1990, JPL Publication 90-54, 243-270.

Graetz, R.D., and Gentle, M.R., (1982), The relationship between reflectance in the Landsat wavebands and the composition of an Australian semi-arid shrub rangeland, *Photogramm. Eng. Remote Sens.*, 48(11): 1721-1730.

Green, R.O., Conel, J.E. and Roberts, D.A., 1993, Estimation of Aerosol Optical Depth and Additional Atmospheric Parameters for the Calculation of Apparent Surface Reflectance from Radiance Measured by the Airborne Visible-Infrared Imaging

Spectrometer (AVIRIS), *Summaries of the 4th Annual JPL Airborne Geoscience Workshop, Oct 25-29,* Vol. 1. AVIRIS Workshop, Washington D.C., 73-76.

Hanes, T., (1977), California chaparral, In *terrestrial vegetation of California*, (M.G. Barbour and J. Major Eds., Calif. Native Plant Soc. Spec. Publ., 9. pp. 417-440.

Huete, A.R. (1986) Separation of soil-plant spectral mixtures by factor analysis, *Rem. Sens. Environ,* 19:237-251.

Johnson, P.E., Smith, M.O., Taylor-George, S., and Adams, J.B. (1983), A semiempirical method for analysis of the reflectance spectra of binary mineral mixtures, *J. Geophys. Res.*, 88: 3557-3561.

Keeley, J.E., and Keeley, S.C., (1988), Chaparral, In North American Terrestrial Vegetation, (M.G. Barbour and W.D. Billings, Ed.), Cambridge University Press, NY, Chap. 6, pp. 165-208.

Nichols, J., (1974), Mapping of the wildland fuel characteristics of the Santa Monica Mountains of California, Final Report to: Riverside Fire Laboratory, UC-USFS Coop Agree. No. 21-274. Nov, 1984, 74 pp.

Norris, R.M., and Webb, R.W. (1990), Geology of California, 2nd Edition, John Wiley and Sons, Inc., 541 pp.

Office of Emergency Services (1995), Santa Monica fire history maps, 1935 to 1954, 1954 to 1974 and 1974 to 1994, Joint OES-FEMA Disaster Field Office, 245 S. Los Robles Ave., 4th floor, Pasadena, CA, 91101.

Pech, R.P., Graetz, R.D., and Davis, A.W., (1986), Reflectance modeling and the derivation of vegetation indices for an Australian semi-arid shrubland, *Int. J. Remote Sens.*, 7(3): 389-403.

Radtke, K.W. H., Arndt, A.M., and Wakimoto, R.H., 1982, Fire history of the Santa Monica Mountains, in Proc. Symp. Dynamics and Management of Mediterranean-type Ecosystems. San Diego, Ca, USFS General Technical Report PSW-58: 438-443.

Ray, T.W., and Murray, B.C., (1996), Nonlinear spectral mixing in desert vegetation, *Remote Sens. Environ.* 55:59-64.

Roberts, D.A., Smith, M.O., Sabol, D.E., Adams, J.B. and Ustin, S., 1992, Mapping the Spectral Variability in Photosynthetic and Non-Photosynthetic Vegetation, Soils and Shade using AVIRIS, *Summaries 3rd Annual JPL Airborne Geoscience Workshop: Vol. 1, AVIRIS,* Pasadena, CA. June 1 and 2, 1992, pp. 38-40.

Roberts, D.A., Adams, J.B., and Smith, M.O., 1993, Discriminating Green Vegetation, Non-Photosynthetic Vegetation and Soils in AVIRIS Data, *Rem. Sens. Environ.*, 44: 2/3 255-270.

Roberts D.A., Green, R.O., and Adams, J.B., 1996, Temporal and spatial patterns in vegetation and atmospheric properties from AVIRIS, submitted, *Rem. Sens. Environ.*,

Sabol, D.E., Adams, J.B., and Smith, M.O., 1992, Quantitative sub-pixel spectral detection of targets in multispectral images, *J. Geophys. Res.* 97: 2659-2672.

Shasby, M.B., Burgan, R.E, and Johnson, G.R. (1981), Broad area forest fuels and topography mapping using digital Landsat and terrain data et al., In *Proc. 7th int. Symp. Machine Process. Remotely Sens. Data.*, Purdue Univ., p. 529-538.

Shimabukuro, Y.E., Holben, B.N., and Tucker, C.J., (1994), Fraction images derived from NOAA AVHRR data for studying the deforestation in the Brazilian Amazon, *Int. J. Remote Sens.* 15:517-520.

Shipman H., and Adams, J.B., (1987), Detectability of minerals in desert alluvial fans using reflectance spectra, *J. Geophys. Res.* 92(B10): 10391-10492.

Smith, M.O., Ustin, S.L., Adams, J.B., and Gillespie, A.R., 1990a, Vegetation in deserts: I A regional measure of abundance from multispectral images, *Remote Sens. Environ.*, 31: 1-26.

Smith, M.O., Ustin, S.L., Adams, J.B., and Gillespie, A.R., 1990b, Vegetation in deserts: II Environmental influences on regional abundance, *Remote Sens. Environ.*, 31: 27-52.

Ustin, S.L., Scheer, G., Castaneda, C.M. , Jacquemoud, S., Roberts, D., and Green, R., 1996, Estimating canopy water content of chaparral shrubs using optical methods, this volume.

Wieslander, A.E., and Gleason, C.H., (1954), Major brushland areas of the Coastal Ranges and Sierra Cascades Foothills in California, USDA Forest Service, California Forest and Range Experiment Station miscellaneous paper 15.

Yool, S.R., Eckhardt, D.W., and Cosentino, M.J., 1985, Describing the brushfire hazard in southern California. *Anal. Assoc. Am. Geograph.* 75: 431-442.

Table 1: Two-endmember mixture models. Note, pixels were assigned to each class in the order listed below. Where overlap occured, the pixel was assigned to the first model. Spectra described with a (UW) are from the University of Washington collection.

Class	EM1	Type	Pixels*	Description
1	Scpnls	NPV	16371	Litter (UW)
2	Zercist710	NPV	2798	Stems of Eriogonum cinereum
3	Wplph2	NPV	12837	Litter (UW)
4	Cceol2_3410	NPV	17777	Stems of Ceanothus oliganthus
5	Zarca1r2457	NPV	16943	Leaf of Artemisia californica (October)
6	Cadfa_1267	NPV	9188	Stem from Adenostoma fasciculatum
7	Dimbark6	NPV	2300	Bark from tropical tree species (UW)
8	Sophora	GV	33731	Leaf (UW)
9	Z1bmala10b	GV	12120	Leaf from Malosma laurina, (October)
10	Grassme1	GV	40628	Grass spectrum (UW)
11	Qudo1stack	GV	3498	Leaf stack from Quercus douglasii (UW)
12	Blkbrush	GV	2950	Leaves from Coleogyne ramossisima
13	Ogheather	GV	3641	Leaf (UW)
14	Buro0	GV	3181	Ambrosia dumosa (UW Collection)
15	Azg2	Soil	1158	Soil, (UW)
16	Az30a284	Soil	515	Soil, (UW)
17	Dcrs3	Soil	351	Soil, (UW)
18	Az10284	Soil	743	Soil, (UW)
19	Hg185a	Soil	1590	Soil, (UW)
20	Wplph2	NPV	1165	Litter (UW)
21	Scrs5	Soil	211	Soil (UW)
22	Plss2	NPV	349	Litter (UW)
23	Purglan	GV	529	Purshia glandulosa (UW)
24	Zarca1st245	NPV	1014	Stem from Artemisia californica
Total Modeled			185,588	
Water			66,656	
Unmodeled			62,124	

Table 2.0 Three-endmember mixture models. Note, all pixels modeled by two-endmember models have been masked. As in the two-endmember models, pixels were assigned to each class in the order listed below. Where overlap occured, the pixel was assigned to the first model.

Class	EM1	Type	EM2	Type	Pixels
25	Scpnls	NPV	Plls2	NPV	5205
26	Ogheather	GV	Purglan	GV	8272
27	Cceol2_3410	NPV	Az30a284	Soil	4286
28	Qudo1stack	GV	Az30a284	Soil	5604
29	Wplph2	NPV	Zlbmala10b	GV	21362
30	Plss2	NPV	Purglan	GV	4909
31	Wplph2	NPV	Az10284	Soil	1058
32	Wplph2	NPV	Qudo1stack	GV	825
33	Grassme1	GV	Az10284	Soil	969
34	Zercist710	NPV	Az30a284	Soil	236
35	Azg2	Soil	Purglan	GV	327
36	Dimbark6	NPV	Plls2	NPV	248
Total					55,882
Total 2-em					185,588
Water					66,656
Unmodeled					10,774

Figure Captions

Figure 1. Index map of the study area. Apparent reflectance spectra of chamise, Ceanothus and coastal sage scrub are provided to the left, labeled as Castro, Ceanothus and Zuma. The original scene has been rotated 90° counterclockwise to orient north towards the top of the page.

Figure 2 a) Reflectance spectra of two leaves (Grassme1 and Sophora) and an apparent reflectance spectrum of chamise (Castro). GV-shade mixture models of Castro using the two different leaf spectra. b) Shows a mixture model for chamise, which can be modeled as 52% GV with an RMS of 0.038 using Grassme1 or as 42% GV with an RMS of 0.019 using Sophora. The sophora model produces the smaller residuals.

Figure 3 a) NIR vs red scatterplot showing three spatially and spectrally distinct regions of the image. Candidate two-endmember models are plotted as vectors connecting photometric shade to each endmember. Selection criteria for each model are listed on the right. b) NIR vs SWIR scatterplot for the same data clusters.

Figure 4. Selection of the three two-endmember mixture models. The associated spectra are plotted on the left, the distribution of each is shown on the right, plotted with Scpnls, Sophora and Azg2 as red, green and blue, respectively.

Figure 5. Histograms showing model overlap for two-endmembers (dark) and three-endmembers (light).

Figure 6. Vegetation map of drought deciduous and senesced vegetation generated using the NPV endmembers. A key to the 9 NPV classes is shown on the left. Evergreen vegetation is shown as blue, ocean and unmodeled pixels are shown as black.

Figure 7. Vegetation map of evergreen and urban vegetation generated using the GV endmembers. A key to the 8 GV classes is shown on the left. Senesced and drought deciduous vegetation is shown as blue, ocean and unmodeled pixels are shown as black.

Figure 8. Fraction image showing NPV, GV and soil fractions as red, green and blue, respectively.

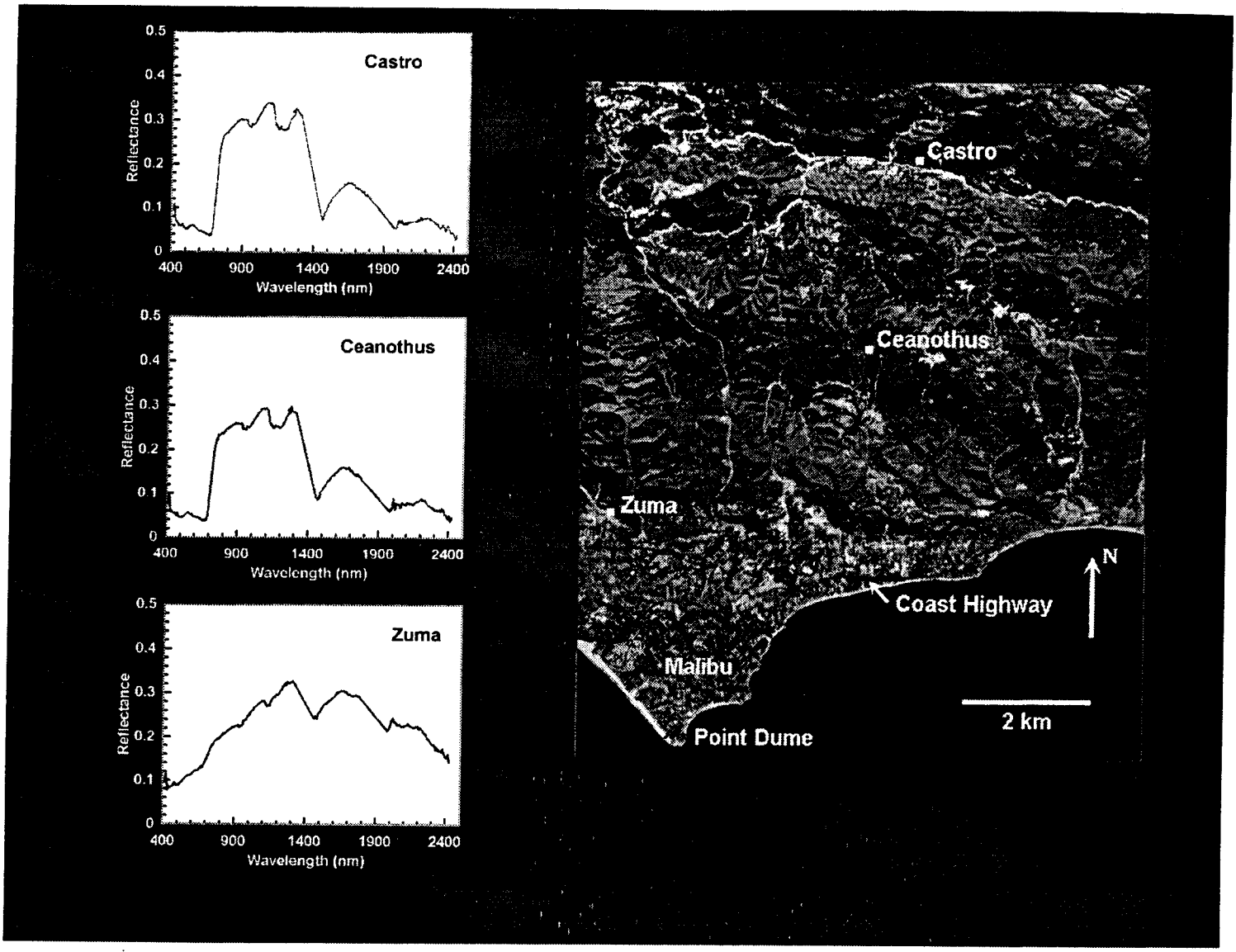

Fig 1, Roberts et al.

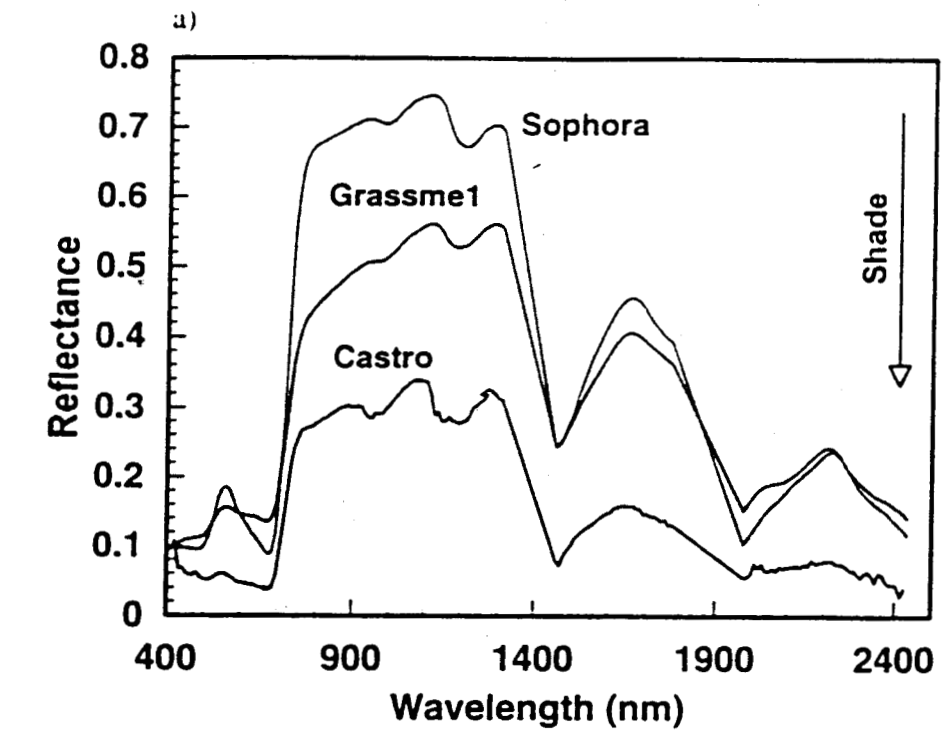
a)
Reflectance
0.8
0.7
0.6
0.5
0.4
0.3
0.2
0.1
0
Sophora
Grassme1
Castro
Shade
400
900
1400
1900
2400
Wavelength (nm)

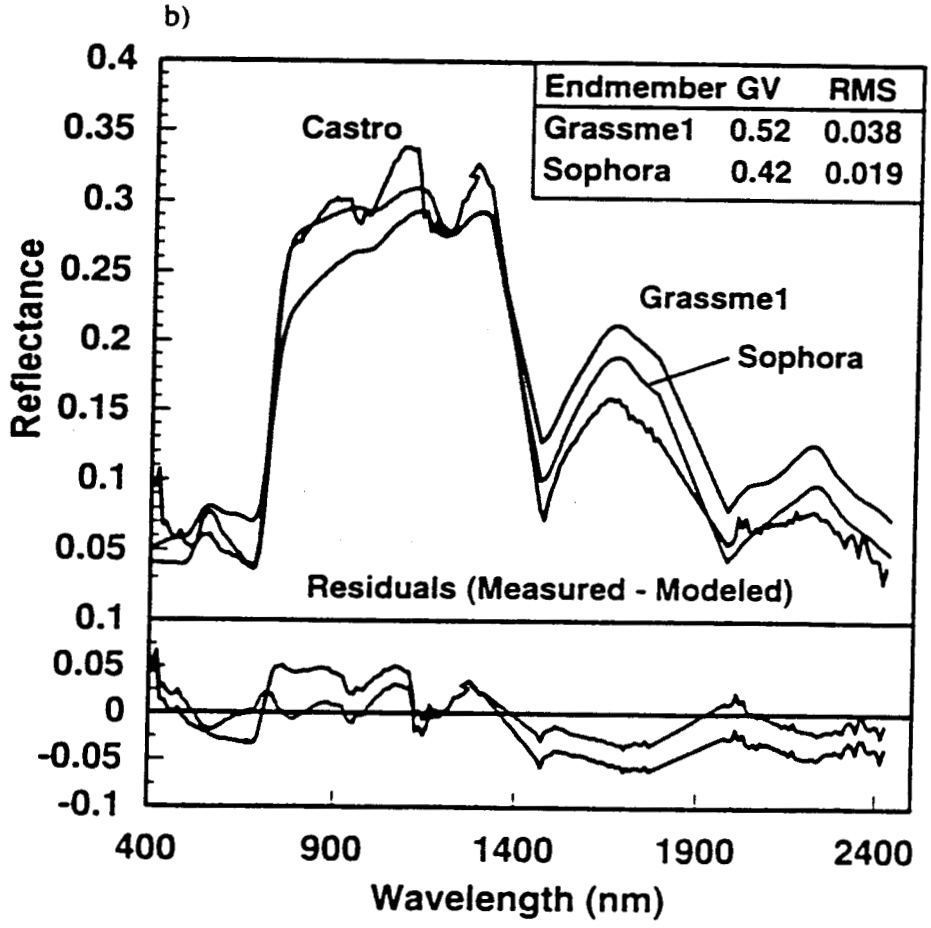
b)
Reflectance
0.4
0.35
0.3
0.25
0.2
0.15
0.1
0.05
Endmember GV RMS
Grassme1 0.52 0.038
Sophora 0.42 0.019
Castro
Grassme1
Sophora
Residuals (Measured - Modeled)
0.1
0.05
0
-0.05
-0.1
400
900
1400
1900
2400
Wavelength (nm)

Figure 2

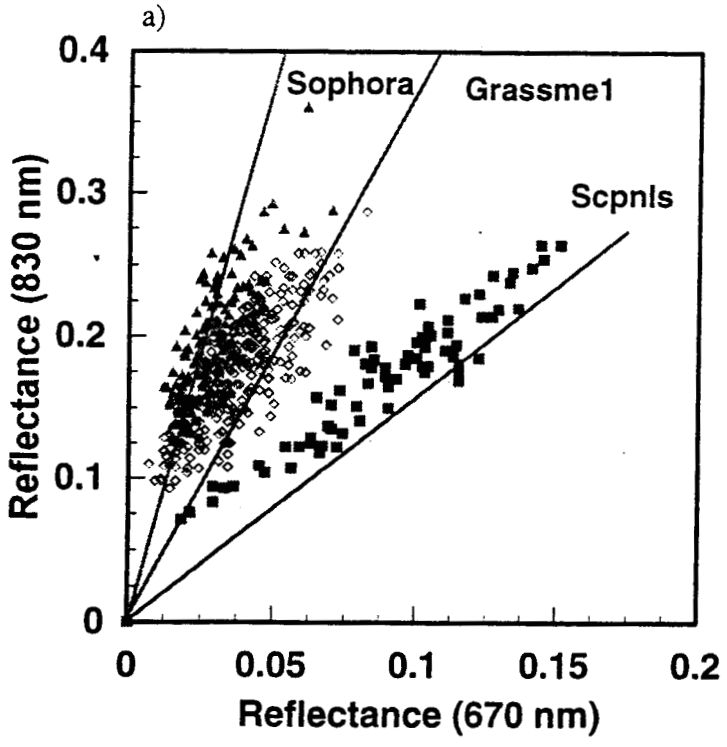

Selection Criteria

Fractions
-0.01 < f < 1.01

RMS
< 0.025

Residual Treshold < 0.025
Threshold Count: 7

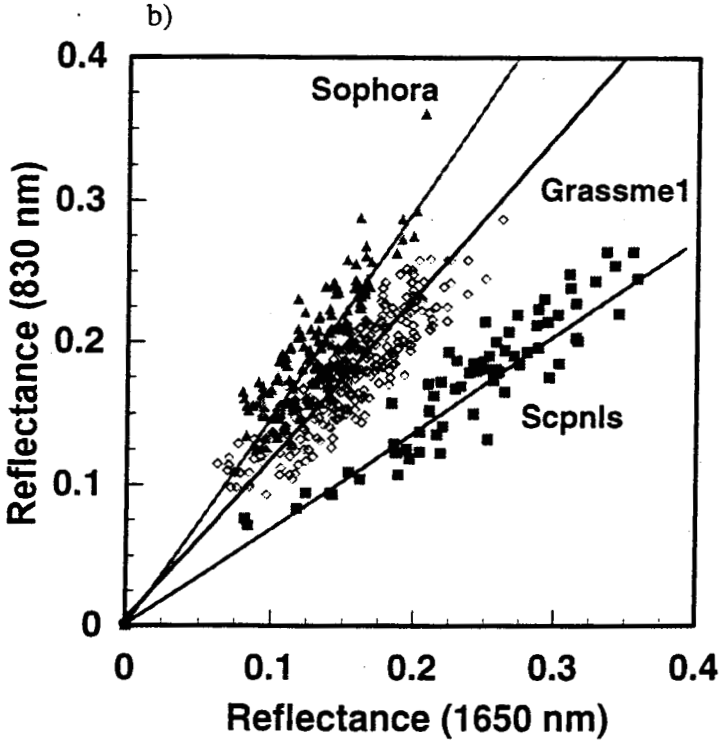

Figure 3

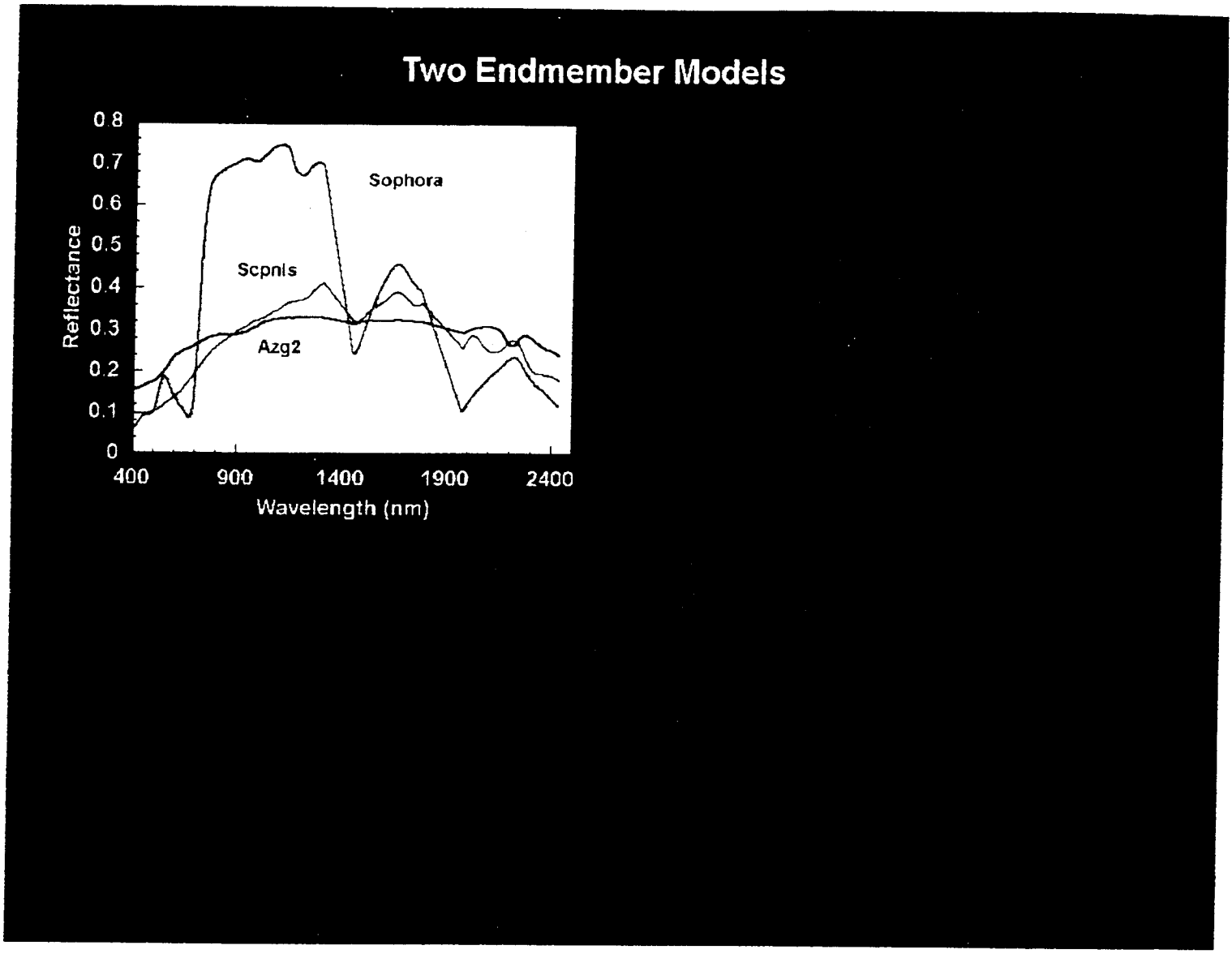
Two Endmember Models
0.8
0.7
0.6
0.5
0.4
0.3
0.2
0.1
0
Reflectance
Sophora
Scpnls
Azg2
400
900
1400
1900
2400
Wavelength (nm)

Fig 4.

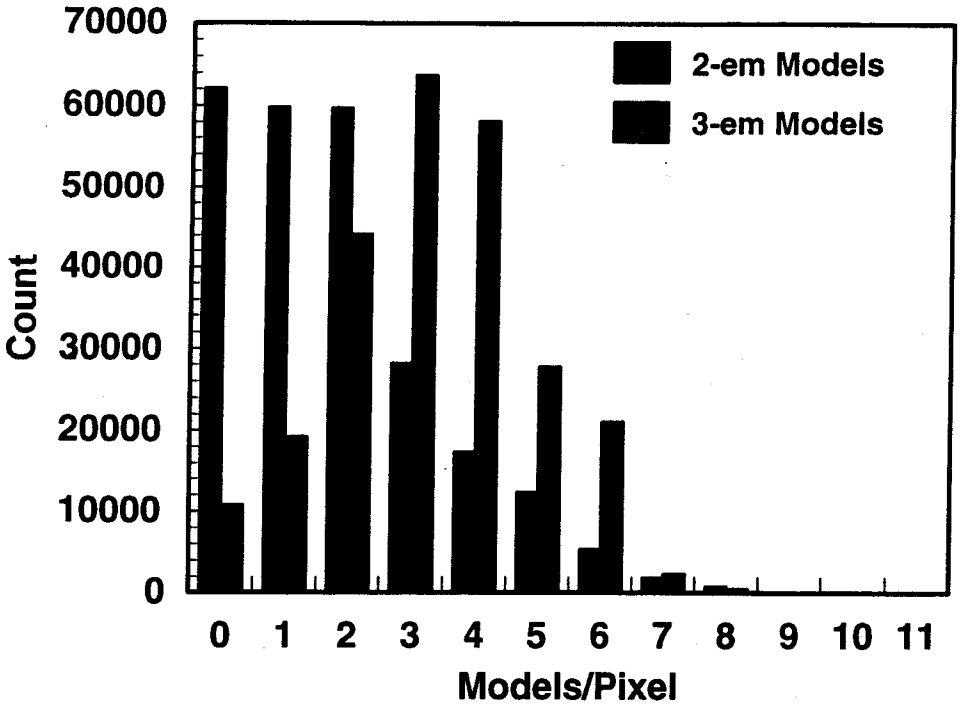
70000
60000
50000
40000
30000
20000
10000
0
Count
2-em Models
3-em Models
0 1 2 3 4 5 6 7 8 9 10 11
Models/Pixel

Figure 5

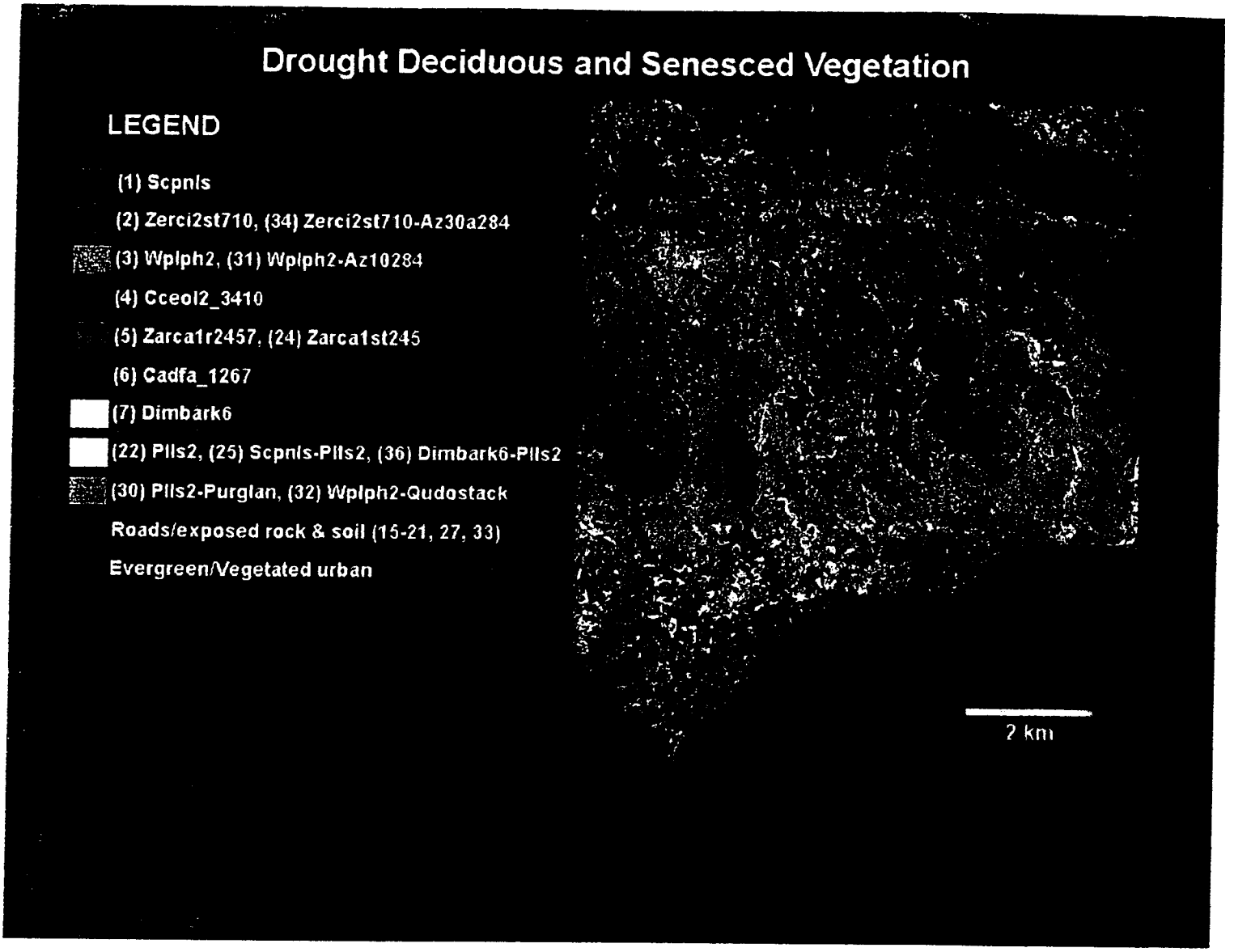
Drought Deciduous and Senesced Vegetation
LEGEND
(1) Scpnls
(2) Zerci2st710, (34) Zerci2st710-Az30a284
(3) Wplph2, (31) Wplph2-Az10284
(4) Cceol2_3410
(5) Zarca1r2457, (24) Zarca1st245
(6) Cadfa_1267
(7) Dimbark6
(22) Plls2, (25) Scpnls-Plls2, (36) Dimbark6-Plls2
(30) Plls2-Purglan, (32) Wplph2-Qudostack
Roads/exposed rock & soil (15-21, 27, 33)
Evergreen/Vegetated urban
2 km

Fig 6

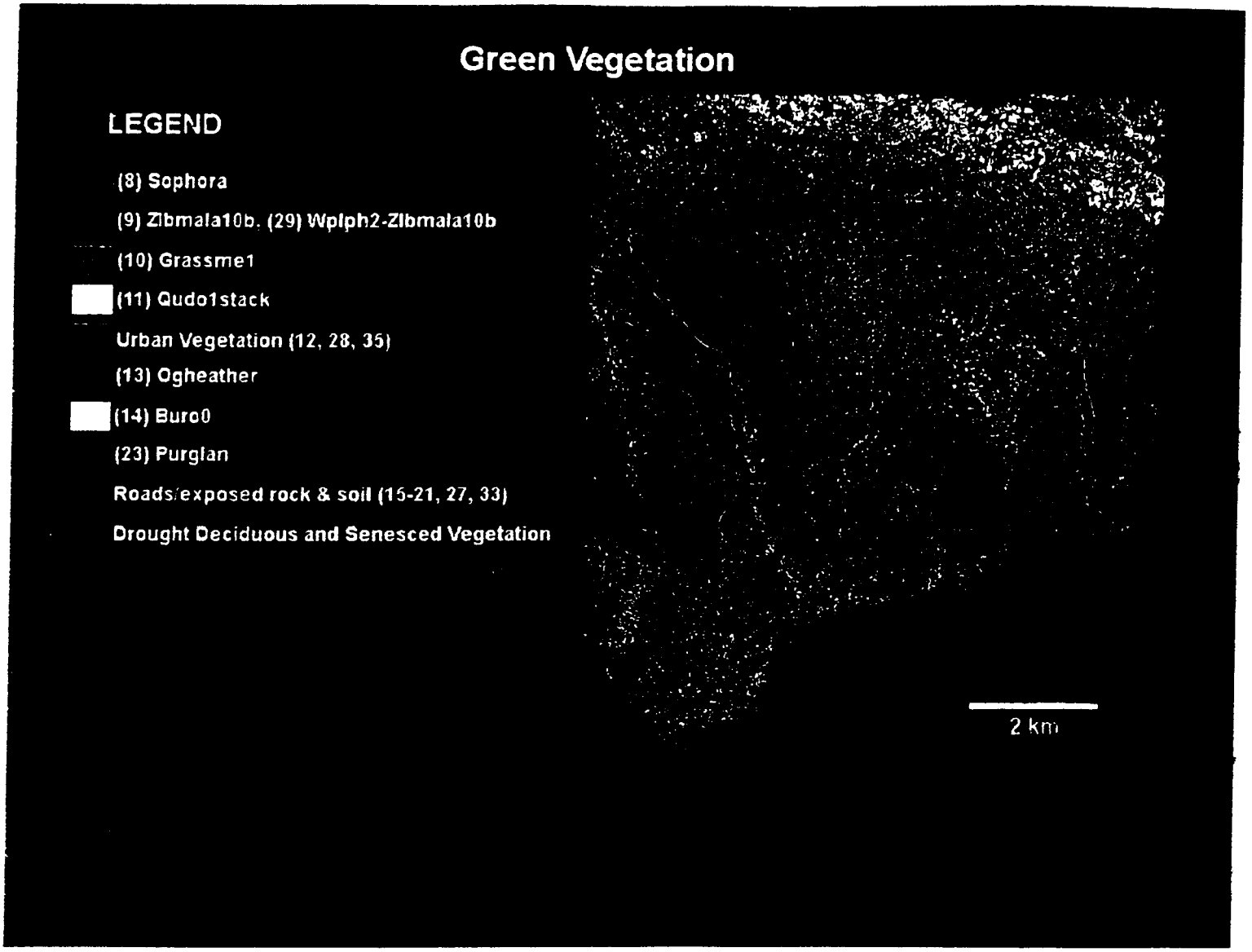
Green Vegetation
LEGEND
(8) Sophora
(9) Zlbmala10b. (29) Wplph2-Zlbmala10b
(10) Grassme1
(11) Qudo1stack
Urban Vegetation (12, 28, 35)
(13) Ogheather
(14) Buro0
(23) Purglan
Roads/exposed rock & soil (15-21, 27, 33)
Drought Deciduous and Senesced Vegetation
2 km

Fig 7.

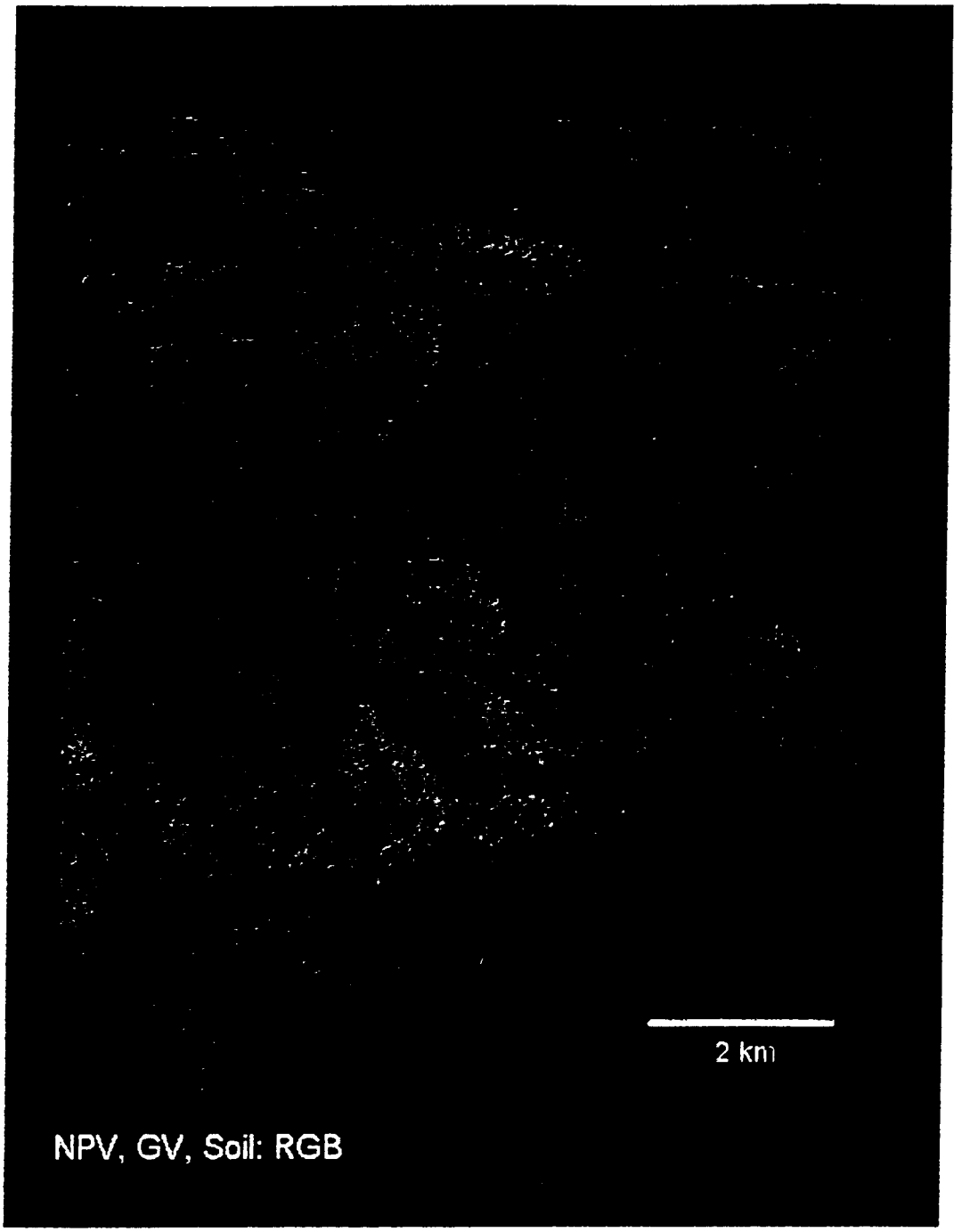

Fig 8